OXFORD

Structural Biology

Mevo lectin specificity toward high-mannose structures with terminal αMan(1,2)αMan residues and its implication to inhibition of the entry of *Mycobacterium tuberculosis* into macrophages

Nukathoti Sivaji[ID][2], **Nikitha Harish**[2], **Samsher Singh**[3], **Amit Singh**[3], **Mamannamana Vijayan**[1,2] and **Avadhesha Surolia**[1,2]

[2]Molecular Biophysics Unit, Indian Institute of Science, Bangalore 560012, India, and [3]Department of Microbiology and Cell Biology, Indian Institute of Science, Bangalore 560012, India

[1]To whom correspondence should be addressed: Tel: +91-80-22932714, 23602763, 23600765, 22932590; Fax: +91-80-23600434; e-mail: mv@iisc.ac.in, surolia@iisc.ac.in

Abstract

Mannose-binding lectins can specifically recognize and bind complex glycan structures on pathogens and have potential as antiviral and antibacterial agents. We previously reported the structure of a lectin from an archaeal species, *Mevo* lectin, which has specificity toward terminal α1,2 linked manno-oligosaccharides. *Mycobacterium tuberculosis* expresses mannosylated structures including lipoarabinomannan (ManLAM) on its surface and exploits C-type lectins to gain entry into the host cells. ManLAM structure has mannose capping with terminal αMan(1,2)αMan residues and is important for recognition by innate immune cells. Here, we aim to address the specificity of *Mevo* lectin toward high-mannose type glycans with terminal αMan(1,2)αMan residues and its effect on *M. tuberculosis* internalization by macrophages. Isothermal titration calorimetry studies demonstrated that *Mevo* lectin shows preferential binding toward manno-oligosaccharides with terminal αMan(1,2)αMan structures and showed a strong affinity for Man-LAM, whereas it binds weakly to *Mycobacterium smegmatis* lipoarabinomannan, which displays relatively fewer and shorter mannosyl caps. Crystal structure of *Mevo* lectin complexed with a Man7D1 revealed the multivalent cross-linking interaction, which explains avidity-based high-affinity for these ligands when compared to previously studied manno-oligosaccharides lacking the specific termini. Functional studies suggest that *M. tuberculosis* internalization by the macrophage was impaired by binding of *Mevo* lectin to ManLAM present on the surface of *M. tuberculosis*. Selectivity shown by *Mevo* lectin toward glycans with terminal αMan(1,2)αMan structures, and its ability to compromise the internalization of *M. tuberculosis in vitro*, underscore the potential utility of *Mevo* lectin as a research tool to study host-pathogen interactions.

Key words: avidity-based interactions, carbohydrate specificity, cross-linking binding mode, *Mevo* lectin, *Mycobacterium tuberculosis* inhibition

Introduction

Lectins are a class of carbohydrate-binding proteins of nonimmune origin and are found in all three kingdoms of life (Drickamer and Taylor 1993; Loris. 2002; Vijayan and Chandra 1999; Sharon 2007; Pérez et al. 2015; Feinberg et al. 2017; Sivaji et al. 2017). They have the ability to specifically recognize and bind carbohydrate structures present on pathogens and have been reported to show antiviral and antibacterial activity (Dam and Fred Brewer 2009; Wesener et al. 2017; Acosta and Lepenies 2019). The glycan structures displayed on the surface of many pathogens frequently play important roles in their transmission and entry into target cells (Vigerust et al. 2007). *Mycobacterium tuberculosis* is a deadly pathogen, responsible for 10.4 million new cases and close to 1.5 million deaths a year (Global tuberculosis report 2019). Many pathogens, including *M. tuberculosis* use high-mannose structures present on their surface to enter into host cells (Ernst 1998; Turner and Torrelles 2018). *M. tuberculosis* primarily establishes infection by invading alveolar macrophages (Mϕs) and dendritic cells (DCs). It has been shown that mannose-binding C-type lectins present on Mϕs and DCs, namely, macrophage mannose receptor (MMR) and DC-specific intercellular adhesion molecule-3-grabbing nonintegrin (DC-SIGN) help *M. tuberculosis* to invade Mϕs and DCs, respectively. Most pathogenic mycobacterium species including *M. tuberculosis* harbor mannosylated structures, such as cell-surface glycolipids, phosphatidylinositol mannosides (PIMs) and mannose-capped lipoarabinomannan (ManLAM) on their cell surface. *M. tuberculosis* infects host Mϕs and DCs by ligation of MMR and DC-SIGN via the mycobacterial surface-exposed ManLAM and PIMs (Schlesinger 1993; Tailleux et al. 2003; Torrelles et al. 2006; Ehlers 2010).

Many mannose-binding lectins from plant and other sources are shown to have antiviral and antibacterial activity by recognizing the high-mannose structures (Driessen et al. 2012; Covés-Datson et al. 2020; Lusvarghi and Bewley 2016; Mitchell et al. 2017). A number of mannose-binding lectins are shown to have anti-HIV activity by recognizing the high-mannose structures present on GP140/GP120 thus neutralizing HIV (Ziółkowska et al. 2006; Akkouh et al. 2015; Mazalovska and Kouokam 2018; Jayaprakash et al. 2020). One such lectin, cyanovirin-N (CV-N), has been reported to reduce the infectivity of the Ebola, Hepatitis C and HIV-1 viruses by targeting surface-exposed mannosylated proteins (Boyd et al. 1997; Tsai et al. 2004; Xiong et al. 2010). A study investigated the ability of CV-N to inhibit *M. tuberculosis* infection, since *M. tuberculosis* also expresses mannosylated structures on its surface. Surprisingly, despite having mannosylated structures on both Mϕs and DCs, CV-N competed with the C-type lectins, DC-SIGN and mannose receptor for ligand binding and inhibited the binding of *M. tuberculosis* to DCs but not to Mϕs (Driessen et al. 2012). However, many of these antiviral or antibacterial lectins show cytotoxicity/mitogenicity, making them less attractive therapeutics (Borrebaeck and Carlsson 1989; Huskens et al. 2008; Singh et al. 2014).

Studies on microbial lectins are few and far between compared to those from plants and animals, although there have been important studies on a few prokaryotic lectins (Boyd et al. 1997; Jayaraman et al. 2005; Kaus et al. 2014). One focus in our laboratory has been on mycobacterial lectins and recently we extended our efforts to investigation on lectins from archaeal species (Patra et al. 2014, 2016, Abhinav et al. 2013, 2016). We previously reported a mannose-binding lectin, *Mevo* lectin, from an archaeal species with an unusual heptameric structure and its interactions with manno-oligosaccharides (Sivaji et al. 2020). Here, we present crystallographic, solution and functional studies on interactions of *Mevo* lectin with high-mannose

structures having αMan(1,2)αMan at the nonreducing end. *Mevo* lectin showed high specificity toward a mannotetrose (Man4) and a mannoheptose (Man7D1) with αMan(1,2)αMan at the nonreducing end. These oligosaccharides are the terminal part of the glycans which are abundantly present on many pathogens including *M. tuberculosis* (Turner and Torrelles 2018). Additionally, *Mevo* lectin shows exquisite specificity toward the *M. tuberculosis* lipoarabinomannan (ManLAM) compared to *Mycobacterium smegmatis* lipoarabinomannan (MsmLAM). Our functional studies demonstrate that *Mevo* lectin affects the *M. tuberculosis* internalization by Mϕs. It does so by interacting with mannosylated caps of ManLAM on the cell-surface. Taken together, these studies reveal the specificity of *Mevo* lectin toward the terminal αMan(1,2)αMan containing manno-oligosaccharides. Its efficacy against *M. tuberculosis* in vitro and its noncytotoxic nature highlights its potential as a research tool and paves the way to test its efficacy in animal challenge models.

Results and discussion

Determination of affinity for manno-oligosaccharides (Man4 and Man7D1) and glycans with terminal αMan(1,2)αMan by isothermal titration calorimetry

Previously, isothermal titration calorimetry (ITC) was used to characterize the binding of *Mevo* lectin to mannose, two dimannoses, 1 trimannose and 1 pentamannose, and the results showed that it binds to mannose and mannose-containing sugars (branched manno-oligosaccharides with 1,3 and 1,6 linkages) with millimolar affinity (Sivaji et al. 2020). We have now extended this analysis to study a larger branched oligomannose, mannoheptose (αMan(1,2)αManα(1,2)αMan(1,3)[αMan(1,3)[αMan(1,6)]αMan(1,6)]αMan; referred to as Man7D1) with a αMan(1,2)αMan(1,2)-αMan structure (D1 arm), αMan(1,3)αMan(1,6)αMan (D2 arm) and a single αMan (D3 arm) at its nonreducing ends (Fig 1A). Plot of incremental heats evolved as a function of the molar ratio of the ligand to the protein (Fig 1B) could not be fitted satisfactorily using a single set of sites for the reaction (Fig 1C). However, ITC curves could be fitted to two sets of sites binding model (Fig 1D). The two sets of sites differ from each other in their binding affinity for Man7D1 by 50-fold, suggesting that the two arms of Man7D1 interact with the binding sites with varying tenacity on the subunits located in the adjacent/symmetry-related heptamers observed in the crystal structure. A cooperative effect appears to contribute to the observed enhancement in the affinity of Man7D1, in addition to the extended interactions noted for the D1 arm of Man7D1 in the secondary site of *Mevo* lectin by X-ray crystallographic studies discussed later. ITC data reported earlier for mannotriose and mannopentose, in contrast, could be fitted to a single set of sites though their αMan1,3 and αMan1,6 ends too occupy binding sites on the adjacent/symmetry-related heptamers. This is not surprising as both mannotriose and mannopentose interact with the lectin through their nonreducing end terminal mannosyl residues only. The high and low affinity sites of Man7D1 show values of binding constants that are 6.6×10^4 ($1.4 \times 10^7 M^{-1}$) and 1.1×10^3 ($2.5 \times 10^5 M^{-1}$) times stronger than that observed for mannotriose/mannopentose, respectively (Sivaji et al. 2020).

The striking enhancement in the affinity for Man7D1 over that observed for mannotriose or mannopentose appears to be related to the oligomeric nature together with the unusual supra-molecular architecture of the *Mevo* lectin-branched manno-oligosaccharide complexes. A careful examination of the complexes of *Mevo*
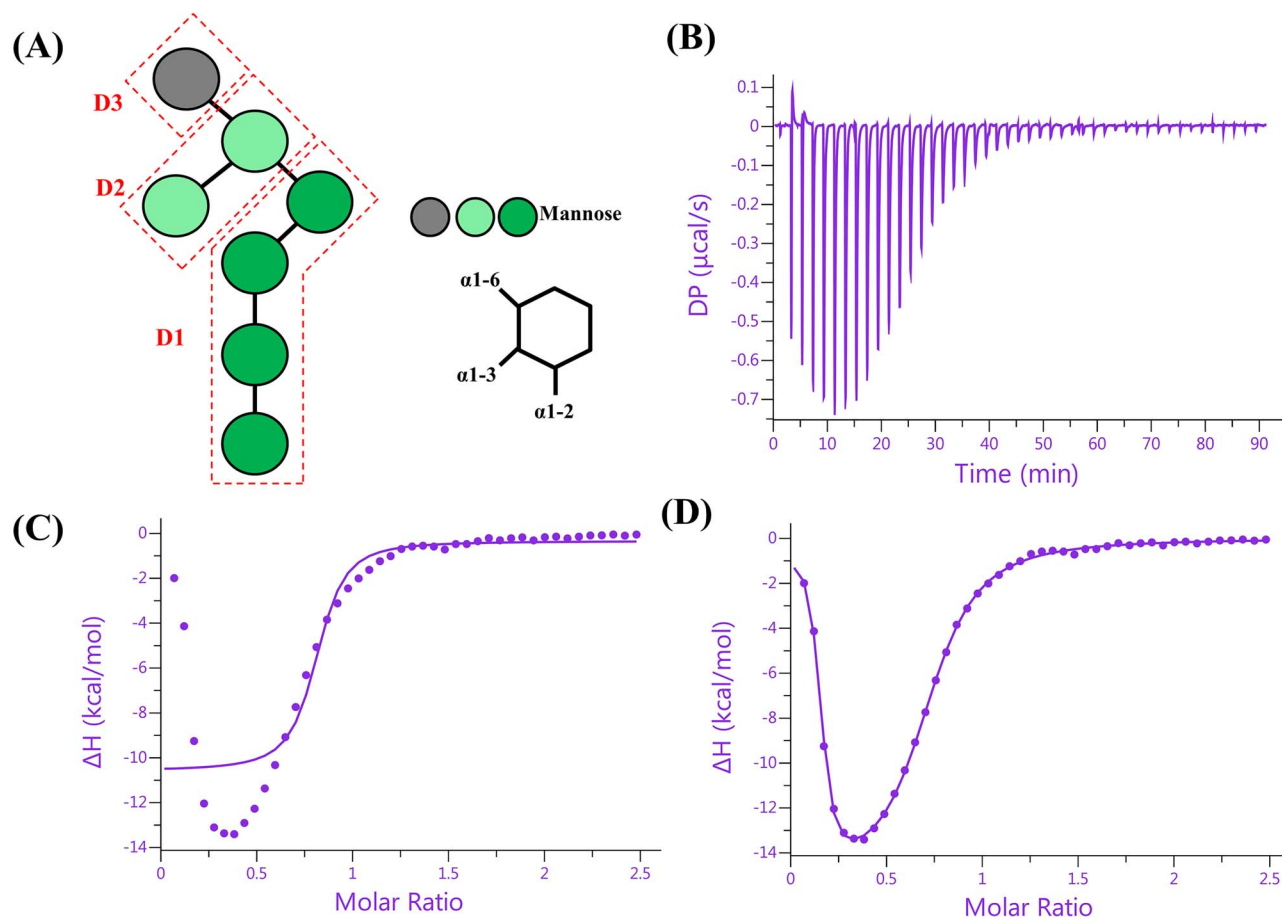
Fig. 1. (A) Schematic diagrams of Man7D1. Key defining linkages between mannose residues (adopted from Feinberg et al. 2017) are given on the right. Shown in green are the mannose residues for which the electron density is well defined in the crystal structure of the Man7D1 complex. D1, D2 and D3 arms of Man7D1 are labeled. **(B)** Isothermal titration calorimetry (ITC) data for Man7D1. Heats evolved upon incremental addition of successive injections of Man7D1 solution (1 mM) to protein (100 μM) in the ITC cell at 25°C. Plots of total heat released as a function of the molar ratio of Man7D1 to protein for the above titration using **(C)** single set of sites and **(D)** two sets of sites.

lectin with mannotriose, mannopentose and mannoheptose, along with the thermodynamic parameters reveals that the existence of three, four and six cross-links, respectively, in the complexes is accompanied by a progressive gain in entropies which amount to 1.77, 2.52 and 5.4 kcal mol^{-1} over the average value of the change in entropy observed in the interactions of the two mannodisaccharides examined (Supplementary Table SI). This in turn suggests that a restriction of conformational mobility plays a key role in the observed thermodynamics of lectin-branched oligosaccharides complexes investigated. This is related to the effort involved in the formation of cross-linked complexes of defined stoichiometry and geometry from variously liganded heptamers floating free in solution and their consequent stabilization by cross-linking. This most likely results in a positive ΔS value. The observation of a positive change in entropy is often associated with predominance of nonpolar interactions in the stabilization of protein-ligand complexes in aqueous solution (Sturtevant. 1977; Tanford. 1980). It can be discounted for the binding of manno-oligosaccharides to the *Mevo* lectin as no appreciable nonpolar interface is seen in the interaction of Man7D1 and *Mevo* lectin in X-ray crystal structure. A diminution in the change in entropy (+ΔS) has sometimes been ascribed to ligand distortion or restriction of conformational mobility of the ligand (Imberty and Pérez 2000; Zierke et al. 2013; Abhinav et al. 2015). As there is

no precedence in the literature on the thermodynamic parameters for the association of branched oligosaccharides with propensity for forming highly ordered cross-linked complexes with highly oligomeric carbohydrate receptors like *Mevo* lectin, our conclusions for the observed parameters appear qualitatively consistent with a deterministic role of orientation factor related to the restriction of the conformational mobility of *Mevo* lectin-Man7D1 complex in modulating these interactions. In the structure of the complex of *Mevo* lectin-Man7D1 many more contacts are observed for the interaction involving its D1 arm. To validate that is indeed the case we studied the interaction between Manα(1,2)Manα(1,2)Manα(1,3)Man (Man4) comprising its D1 arm. ITC studies shown in Figure 2 for the binding of Man4 to the lectin give K$_d$ values of 27.8 μM as compared to 12.6 mM for Manα(1,3)Man that constitutes the D2 arm of this heptamannosaccharide, reflecting enhanced interactions of the former in the combining site. Additionally, a cooperative effect as a consequence of cross-linking of Man7D1 to subunits across the adjacent heptamers increases several orders of magnitude, the affinities of both the arms of Man7D1 for binding to their respective sites in the lectin.

Since *Mevo* lectin interacts preferentially with terminal αMan1,2 linked manno-oligosaccharides, its interaction with glycans such as a mannose capped lipoarabinomannan from *M. tuberculosis* (Man-
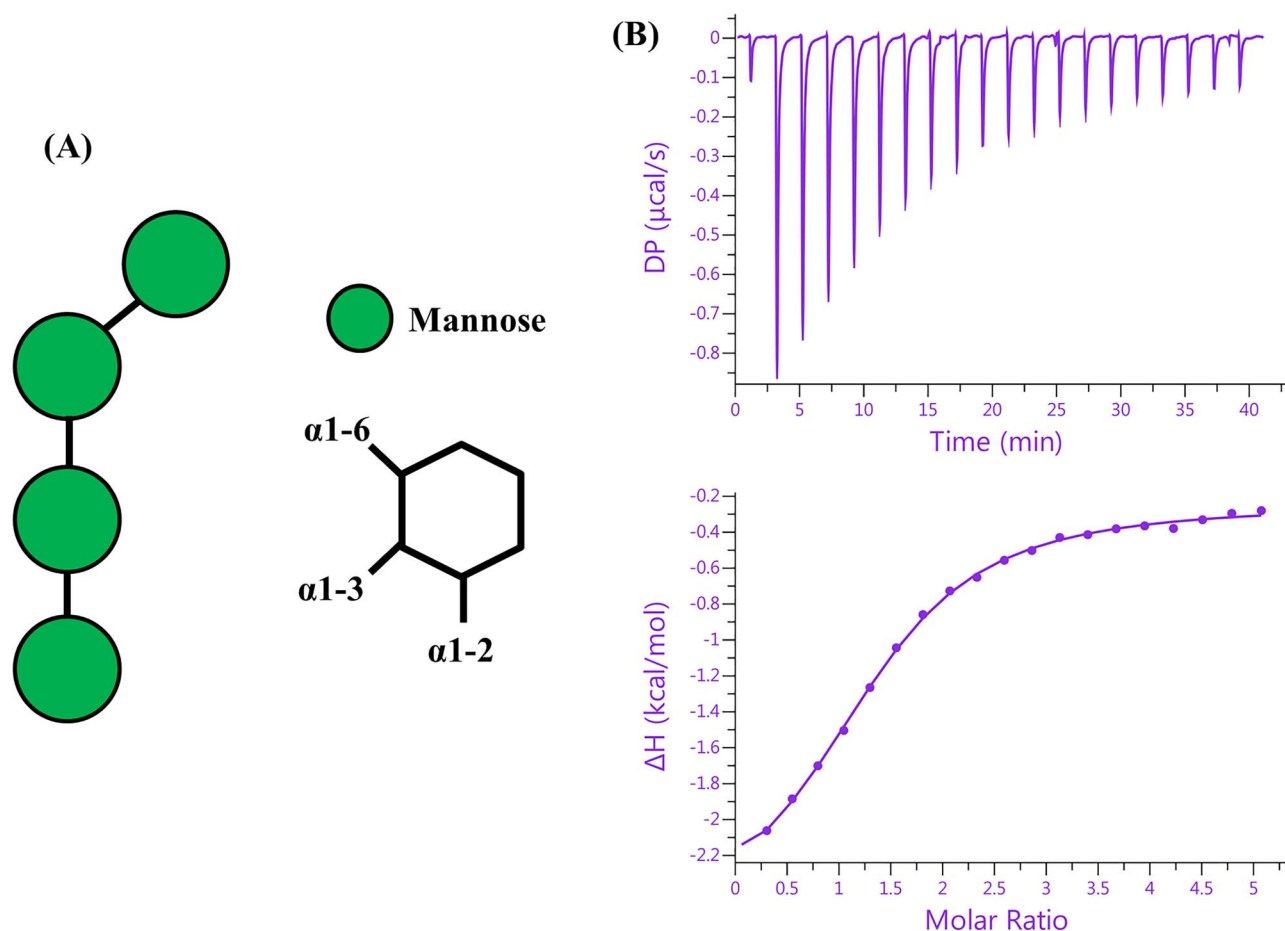
Fig. 2. (A) Schematic representation of Man4. Key defining linkages between mannose residues are given on the right. **(B)** Isothermal titration calorimetry (ITC) data for Man4. Heats evolved upon incremental addition of successive injections of Man4 solution (2 mM) to protein (100 μM) in the ITC cell at 25°C. The plot given below represents total heat released as a function of the molar ratio of Man4 to protein for the above titration using single set of sites.

LAM) and lipoarabinomannan from *M. smegmatis* (MsmLAM) was examined for their binding to *Mevo* lectin. ManLAM carries several branches of $\alpha 1,2$ linked manno-oligosaccharides typically made up of one to four mannose residues referred to as "mannose caps", substituting an arabinan core (Fig 3A). Modeling studies show that $\alpha 1,2$ linked manno-oligosaccharides caps found in ManLAM can readily be accommodated in the binding site of *Mevo* lectin (Fig 3C). Following the modeling studies, the binding of mycobacterial LAMs, ManLAM and MsmLAM (Fig 3B) to the lectin was studied using ITC experiments (Fig 3D,E). ManLAM showed a very high affinity, whereas MsmLAM bound relatively very weakly. ManLAM showed a binding constant (K_a) value of 1.24×10^8 M^{-1}, which is almost a million fold higher than that observed for mannotriose and mannopentose. MsmLAM on the other hand, showed very weak binding to *Mevo* lectin with K_a value of 3.57×10^4 M^{-1} which is 3000-fold less compared to ManLAM (Table I). The stoichiometry (n) and the heat release pattern in the ITC experiments for the larger oligosaccharides pointed to possible differences in complex formation between Man7D1 and mycobacterial LAMs. A value of n equal to 0.25 for MsmLAM and 0.11 for ManLAM suggested that they can interact with four and seven subunits of *Mevo* lectin simultaneously. The fact that the separation between the adjacent carbohydrates binding sites in the *Mevo* lectin heptamer is ~ 35 Å that is complementary to the distance between the successive man-

nose caps in ManLAM perhaps gives rise to the strong and specific *Mevo* lectin-ManLAM interactions. Since the mannosyl caps decorate a highly flexible polysaccharide backbone in ManLAM, there is no conformational restriction to its mobility involved in the formation of complex between *Mevo* lectin and ManLAM. The interactions are driven primarily by favorable changes in enthalpies. The slope of the enthalpy-entropy compensation plot for Man7D1 and the larger manno-oligosaccharide structures is ~ 1.2, indicating that a relatively favorable enthalpic contribution accounts for their binding reaction with the lectin (Supplementary Figure S1). Large negative value of changes in the enthalpies for binding of ManLAM suggests a relatively larger increase in the surface area of contact between them and *Mevo* lectin as compared to that for MsmLAM.

A notable difference between ManLAM and MsmLAM is related to fewer and shorter $\alpha 1,2$ linked mannosyl caps in the latter (Turner and Torrelles, 2018). A value of n equal to 0.11 for ManLAM suggests that the geometry of *Mevo* lectin is optimal for its recognition; apparently, all of binding sites of the heptameric lectin interact simultaneously with the mannose caps of ManLAM. This, in turn, accounts for the enormous avidity effect observed for the enhanced affinities of interactions between *Mevo* lectin-ManLAM complexes. Taken together, calorimetric data and crystallographic structural analyses based on *Mevo* lectin-Man7D1 complex (as discussed in the next section) indicate that the avidity of the multisite,
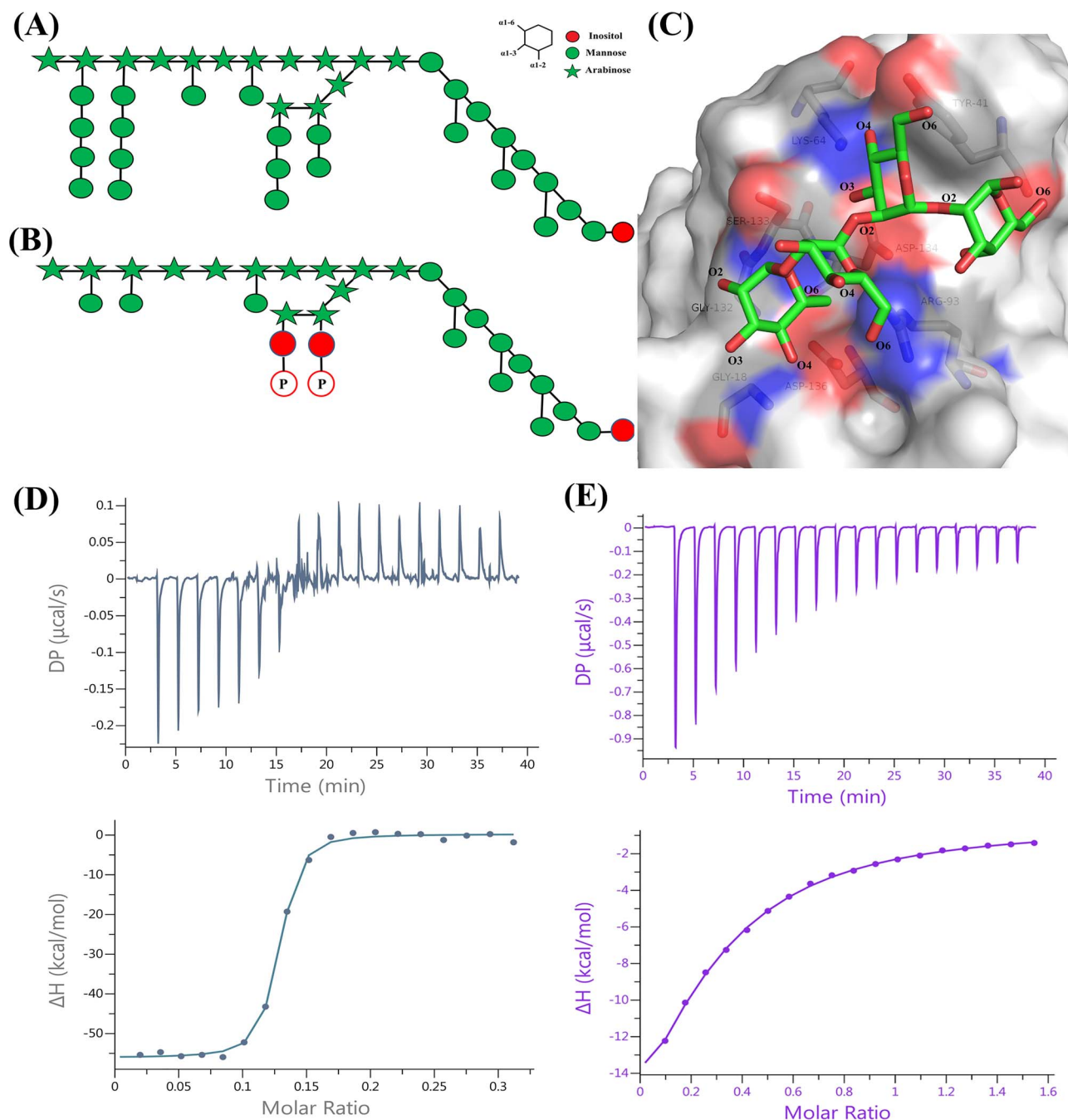
Fig. 3. Schematic of the structure of (**A**) ManLAM and (**B**) MsmLAM. Key to the linkages for the above polysaccharides is provided at the right of panel A. (**C**) The modeled structure of αMan(1,2)αMan(1,2)αMan(1,2)αMan, representing a typical mannose cap from ManLAM. Plot of total heat released as a function of molar ratio of ligand to protein for titrations of *Mevo* lectin with (**D**) ManLAM and (**E**) MsmLAM. The top panel of the figures represents raw data, and the panel below represents the best fit for the obtained data using a single-site model.

multivalent interactions of *Mevo* lectin with the sugars may contribute to its high affinities observed for ManLAM.

Structure of *Mevo* lectin-Man7D1 complex

Mevo lectin is a 7-fold symmetric ring-shaped heptameric molecule (Sivaji et al. 2020). Each subunit has a jacalin-like structure with a β-prism I fold. As expected, the tertiary and the quaternary structure of the molecule, including inter-subunit interactions, is almost the same

as that found in the native crystals used for preparing the complex through soaking. The crystal structure of the complex of Man7D1 with *Mevo* lectin, however, exhibits a subtle difference. The two crystallographically independent molecules in the native structure are related to each other by a noncrystallographic 2-fold axis along the (1 1 0) direction in the tetragonal unit cell. On complexation, this 2-fold axis becomes crystallographic. Consequently, the space group transforms from $P4_12_12$ to $P4_22_12$ with nearly half the **c** dimension (Table II).

Table I. Thermodynamic parameters for the binding of the sugars to *Mevo* lectin at 25°C

	n	K_d (M)	ΔG (kcal mol^{-1})	ΔH (kcal mol^{-1})	$-T\Delta S$ (kcal mol^{-1})
Man4[a]	1.05 ± 0.07	27.8e-6 ± 3.e-6	−6.22 ± 0.1	−3.0 ± 0.1	−3.22 ± 0.3
Man7D1[b]	n_1	K_{d1}	ΔG_1	ΔH_1	$-T\Delta S_1$
	0.77 ± 0.05	2.8e-6 ± 0.4e-6	−7.64 ± 0.1	−14.6 ± 0.1	6.96 ± 0.1
	n_2	K_{d2}	ΔG_2	ΔH_2	$-T\Delta S_2$
	0.15 ± 0.01	37e-9 ± 3.3e-9	−9.36 ± 0.4	0.40 ± 0.7	−9.76 ± 0.7
ManLAM	0.11 ± 0.01	8.15e-9 ± 1.4e-9	−11.0 ± 0.1	−58.3 ± 1.4	47.3 ± 1.4
MsmLAM	0.25 ± 0.15	30.0e-6 ± 7.3e-6	−6.3 ± 0.1	−13.8 ± 0.6	7.5 ± 0.2

[a]αMan(1,2)αManα(1,2)αMan(1,3). [b]αMan(1,2)αManα(1,2)αMan(1,3)[αMan(1,3)[αMan(1,6)]αMan(1,6)]αMan.

Table II. Details of data statistics and refinement

	Man7D1 complex
Space group	P4$_2$2$_1$2
Unit cell dimensions	
a	168.35
b	168.35
c	104.96
(Å)	
α	90.0
β	90.0
γ	90.0
(°)	
No of subunits/asymmetric unit	7
Resolution (Å)	61.18–2.23
	(2.35–2.23)
No. of observations	1410820 (182117)
No. of unique reflections	73523 (10366)
Completeness (%)	99.7 (98)
I/(σI)	7.8 (3.2)
CC(1/2) (%)	98.5 (52.4)
R_{merge} (%)	39.1 (81.3)
Multiplicity	19.2 (17.6)
R_{work} (%)	24.9 (38.1)
R_{free}[a] (%)	26.7 (39.2)
RMS deviations from ideal values	
Bond length (Å)	0.012
Bond angle (°)	1.7
Residues (%) in Ramachandran plot	
Favored region (%)	94.9
Allowed region (%)	5.1
Disallowed region (%)	0

[a]In total, 5% of the reflections were used for the R_{free} calculations. Values in parentheses refer to the highest resolution shells.

Although structures of β-prism I fold lectin complexes with mannose to mannopentose have been examined exhaustively earlier (Jeyaprakash et al. 2004; Singh et al. 2005; Swanson et al. 2015), such studies on higher manno-oligosaccharides seem to be lacking. We describe here the structure of a complex of mannoheptose (αMan(1,2)αManα(1,2)αMan(1,3)-[αMan(1,3)[αMan(1,6)]α Man(1,6)]αMan; referred to as Man7D1) with *Mevo* lectin at 2.23 Å resolution. In the complex, six of the seven mannosyl residues that constitute their D1 and D2 arms, are defined well in the electron density map (Fig 4A,B). They are sandwiched between the reference molecule made up of subunits A–G and a 2-fold symmetric molecule consisting of subunits A′–G′ (Fig 5). The D1 arm occupies the binding site in subunits A, D and G; the D2 arm is located at the binding sites of B′, C′ and F′. To elaborate, A is linked to B′, D–F′ and G–C′. The situation is just the reverse in subunits 'B, C and F' and 'A′, D′ and G''. Electron density exists only for one mannose residue each at the binding sites of subunits E and E′. The remaining residues are presumably disordered. Thus the molecules exist in the crystal structure as symmetric dimers, each apparently stabilized by six crosslinks.

Refinement using appropriate restrains yielded acceptable geometries for the comparatively long oligosaccharide ligands, as evidenced by the values of the relevant torsion angles (Imberty et al. 1990) (Supplementary Table SII). The terminal Manα(1,2)αMan at the nonreducing end plays an important role in the interaction of the ligand with the lectin. The terminal Manα(1,2)αMan in the structures already reported (Sivaji et al. 2020) superpose reasonably well on the corresponding disaccharide residues in the present structure (Fig 6).

The interactions involved in the crosslinks are nearly the same in all the six subunit pairs. Those in one of them are illustrated in Fig 4C. The primary binding site of β-prism I fold lectins is characterized by the G...GXXXD motif. In *Mevo* lectin, the residues involved in the motif are Gly 18, Gly 132, Ser 133, Asp 134, Ile 135 and Asp 136. In the case of previously reported αMan(1,2)αMan complexes, interactions of its nonreducing residue alone with *Mevo* lectin was observed, whereas in its complexes of αMan(1,3)αMan, 30% of the molecules exhibited interactions with the reducing end mannose as well. The interactions of the terminal residues of the D1 and D2 arms for Man7D1, on the other hand, with the primary binding site are nearly the same despite a difference in the linkage of their mannosyl residues. The orientation of the nonreducing end mannosyl residue at the primary binding site directs the C1 atom and much of the ring of the penultimate sugar away from the primary binding site. That in turn places the third mannosyl residue of the D1 arm of the Man7D1 at the secondary binding site defined by Lys 64, Arg 93 and Asp 134. A depiction of D1 arm of Man7D1 in the secondary binding site shows extensive interactions of the innermost/third mannose with residues at this site (Fig 4C). *Mevo* lectin is among the very few β-prism I fold lectins in which Asp (residue 134) occurs at the second X position in the G...GXXXD motif. However, the interactions of Asp 134 with D1 and D2 arms are different for Man7D1. Asp 134 interacts with O4 and O6 of the third mannosyl residue of the D1 arm, whereas the third residue of the D2 arm is such that Asp 134 cannot interact with it in the corresponding (relevant) subunit. Likewise, Lys 64 does not interact with the third residue of the D2 arm in subunits B′, C′ and F′. Arg 93 interacts with it in subunit A′ only. In the view of the above and the extensive interactions
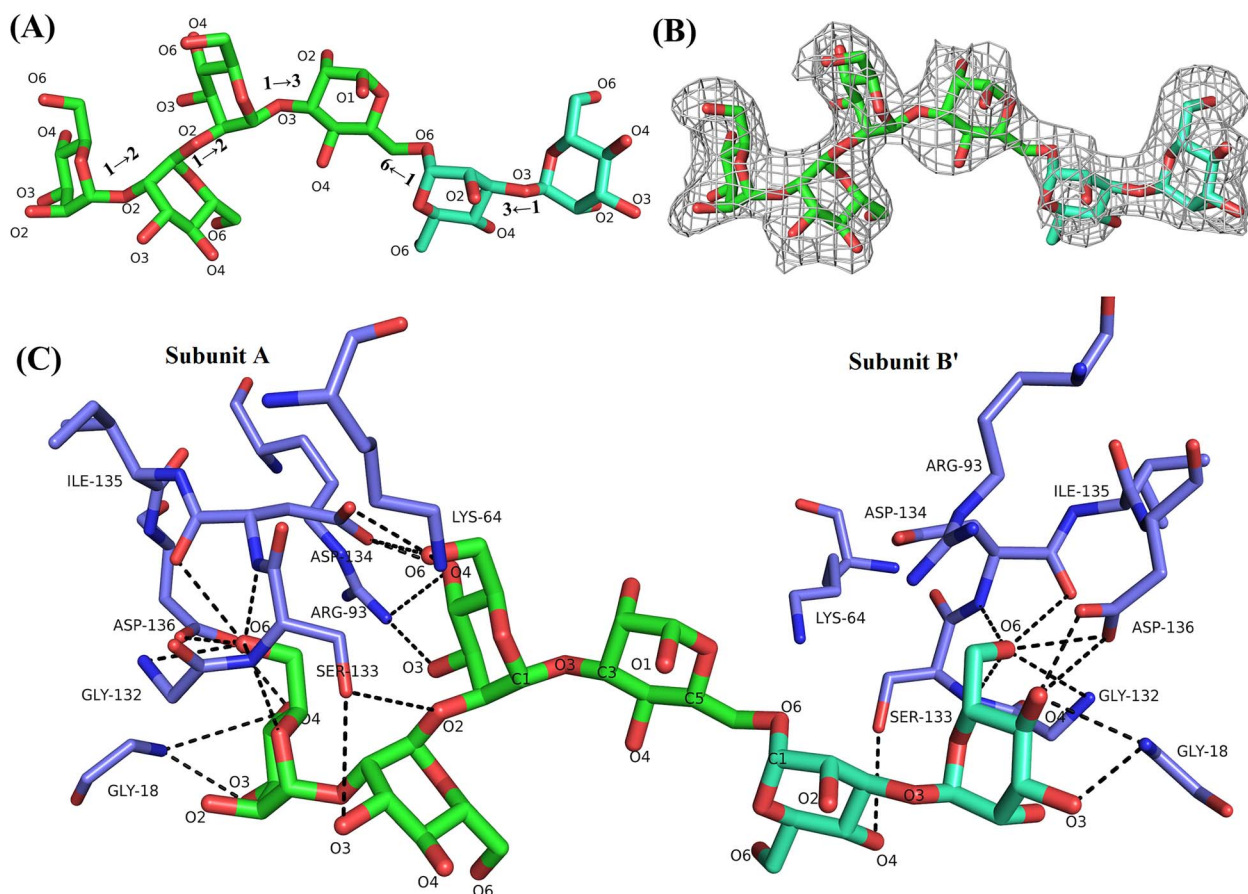
Fig. 4. (A) D1 and D2 arms of Man7D1 shown with linkages. (B) Representative electron density for Man7D1 in simulated annealing F_o-F_c omit map. The map is contoured at 2σ level. (C) Details of interactions of D1 (dark green) and D2 arms (light green) with the residues of the binding site of *Mevo* lectin.

of the third mannosyl residue of the D1 arm with the secondary binding site including the participation of Asp 134 that are absent in the case of D2 arm, one is tempted to suggest that the interactions involving D1 and D2 arm give rise to the high and low affinities, respectively.

The Man7D1 complex also exhibits extensive crosslinking akin to the networks observed in the complexes of mannotriose and mannopentose (Sivaji et al. 2020). Additional features of Man7D1 complex are the interactions at the secondary site with the third mannosyl residue from the nonreducing end, which partly explains the pronounced enhancement of its affinity (1200-fold) compared to that of mannopentose. Mannose, the nonreducing end of the mannose in Manα(1,2)Man, both the reducing and nonreducing ends of mannose in Manα(1,3)Man, both nonreducing end mannose residues in mannotriose and the nonreducing end mannose of α(1,6) branch of mannopentose bind to the site contributed by Gly 18, Gly 132, Ser 133 and Asp 136. The nonreducing end mannose at the α(1,3) branch in mannopentose interacts with a site defined by Tyr 44, Lys 64, Ser 133 and Asp 134. Further, the third mannosyl residue of the D1 arm of Man7D1 that has strong interactions with secondary site involves bifurcated hydrogen bonds between its C4 and C6 hydroxyl and Asp 134 carboxyl groups that contribute significantly to the binding ability of Man7D1. Asp134 carboxyl could partake in similar interaction with the third nonreducing end mannose of Man4. To probe the role of the contributions of Asp 134 to these interactions we mutated it to alanine. ITC studies with D134A,

conducted under identical experimental conditions employed for the wild type protein, show a striking diminution in the binding affinities for both Man7D1 and Man4 underscoring the key role of Asp 134 at the secondary site of *Mevo* lectin for its observed affinity for Man4 and the Man4 bearing arm (D1) of Man7D1 (Supplementary Figure S2). This is not surprising as the hydrogen bond between charged residues such Asp 134 in the combining site of *Mevo* lectin and a hydroxyl group of a sugar is stronger as compared to those between neutral atoms. Further, the hydrogen bond here is being donated by the C4/C6 hydroxyl group of the third mannose from the nonreducing end of D1 arm that is consistent with the fact that the strongest hydrogen bonds in protein-carbohydrate complexes are those where OH serves as the donor rather than acting as an acceptor (Swaminathan et al. 1999).

Cytotoxicity assay

Many mannose-binding lectins that exhibit antiviral and antibacterial properties show mitogenicity/cytotoxicity, limiting their use in antiviral or antibacterial therapy (Huskens et al. 2008; Singh et al. 2014). We, therefore, determined the cytotoxicity of *Mevo* lectin on human kidney HEK293 cells by employing the 3-(4,5-dimethylthiazol-2-yl)-2,5 diphenyltetrazolium bromide (MTT) assay (Kumari et al. 2018). Different *Mevo* lectin concentrations (0 to 5 mg mL^{-1}) were used in the assay. The cytotoxicity of *Mevo* lectin to HEK293 cells after 48 h of exposure is depicted in Figure 7. The results of this experi-
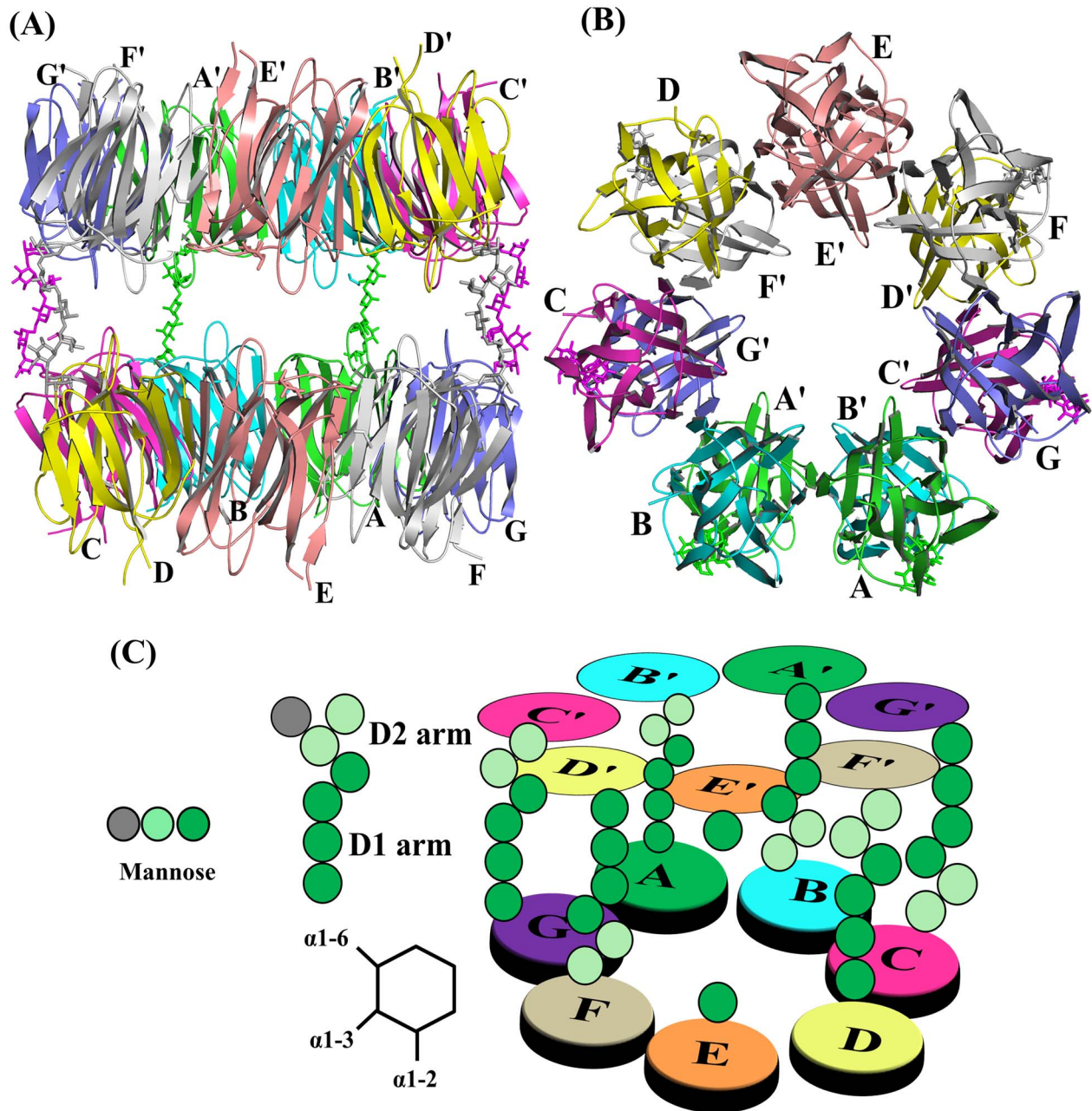
Fig. 5. (**A** and **B**) Symmetric dimer of the *Mevo* lectin molecule complexed with Man7D1 viewed along two directions. The subunits of reference molecule (**A**–**G**) and 2-fold symmetric molecule (**A'-G'**) are marked. (**C**) Schematic representation of cross-linking in the complex involving Man7D1. Shown in dark (D1 arm) and light green (D2 arm) are the mannose residues for which the electron density is well defined in the crystal structure of the Man7D1 complex. Key defining linkages between mannose residues are given at the bottom left. The D1 arm occupies the binding site in subunits A, D and G in the reference molecule, whereas the D2 arm is situated at the binding sites of B', C' and F' in the 2-fold symmetric molecule. The situation is just the reverse in subunits B, C, F and A', D', G'. Only a mannose residue is defined at the binding site of subunit E and E'.

ment demonstrate that *Mevo* lectin did not exhibit any measurable cytotoxicity toward HEK293 cells.

Mevo lectin treatment restrict the invasion of Mϕs by *M. tuberculosis*

Multiple human cell surface receptors are shown to recognize the ManLAM. It is also established that the mannose caps of ManLAM are recognized by MMR, the DC-SIGN and surfactant protein D (Torrelles et al. 2006; Geurtsen et al. 2009). Also, ManLAM interacts with MMR on Mϕs for phagocytic uptake of *M. tuberculosis* (Kang et al. 2005). A few studies have documented the role of lectin binding in preventing mycobacterial or viral entry into the host cells by inhibiting interaction with pattern recognition cell surface receptor(s) (Ji et al. 2005; Tanaka et al. 2009; Driessen et al. 2012; Fukuda et al. 2013). Hence, we investigated whether *Mevo* lectin could
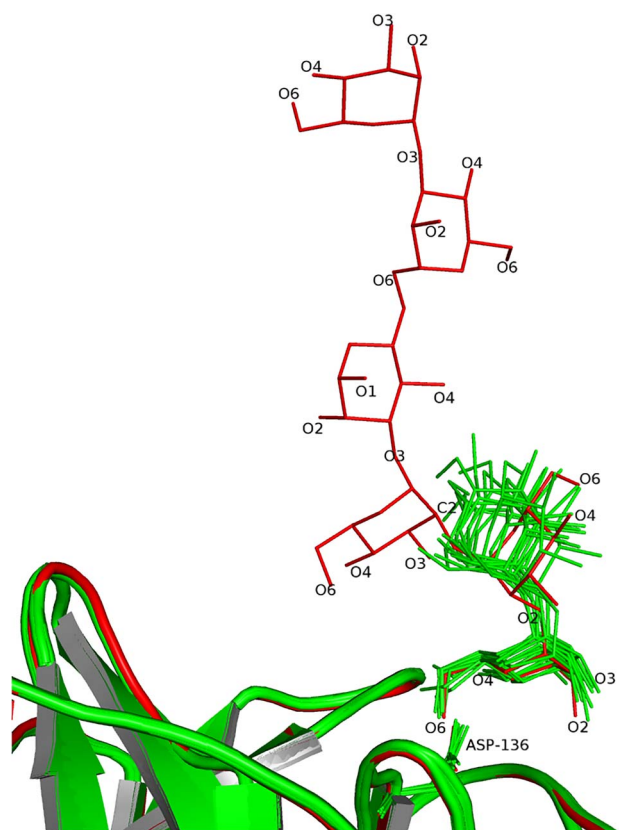
Fig. 6. Superposition of the Manα(1,2)αMan ends (green) in the structures reported earlier (Sivaji et al. 2020) onto the Manα(1,2)αMan end (red) of one of the D1 arm of Man7D1 in the present structure.

block the binding of *M. tuberculosis* to intact Mϕs. Phorbol 12-myristate 13-acetate (PMA)-differentiated THP-1 Mϕs were infected with *Mevo* lectin pretreated fluorescently labeled *M. tuberculosis* and internalization was assessed at 2 h postinternalization. As evident from colony-forming unit (CFU) analysis, when Mϕs were infected at multiplicity of infection (MOI) of 1 or 5, there is 38 or 82% less internalization of *Mevo* lectin treated *M. tuberculosis* as compared to untreated bacilli (Fig 8A), indicating that the binding of *Mevo* lectin interferes with the process of the internalization of *M. tuberculosis*.

As an additional validation, we infected THP-1 Mϕs with a *M. tuberculosis* strain expressing red fluorescent protein (RFP: tdTomato), and fluorescence emitted by the infected Mϕs was scored to estimate internalization. Consistent with our CFU data, tdTomato positive population of *Mevo* lectin treated *M. tuberculosis* (Fig 8B) was 25–30% lesser than that observed for the untreated population, indicating diminished uptake of the bacteria by Mϕs. These data show that a reduced number of bacilli are phagocytosed by Mϕs as a consequence of *Mevo* lectin binding to ManLAM that masks mannosyl moieties to circumvent interaction with MMR.

Conclusions

The specificity of *Mevo* lectin toward manno-oligosaccharides containing αMan(1,2) αMan at their termini has been addressed through crystallographic and solution studies. ITC studies demonstrate that complex manno-oligosaccharides with terminal αMan(1,2) αMan linkages, can bind to *Mevo* lectin with nanomolar affinities.

Structural studies on *Mevo* lectin-Man7D1 complex showed cross-linking similar to that observed in previously reported *Mevo* lectin complexes of mannotriose and mannopentose (Sivaji et al. 2020). Interactions at the primary binding site are mostly similar to those in other β-prism I fold lectins, but substantial additional interactions are made at a secondary site. A detailed analysis of the *Mevo* lectin structure complexed with Man7D1 suggests that the interactions of Asp 134 with the third mannosyl residue of D1 arm, at least partially, contribute to its high-affinity binding. *Mevo* lectin showed no cytotoxicity when incubated with human kidney (HEK93) cells. We demonstrate here that *Mevo* lectin efficiently binds to mycobacterial mannosylated surface lipopolysaccharide (ManLAM) and compromises its ability to infect Mϕs. However, more experiments are needed to be to demonstrate its potential as a bacteriostatic agent.

Materials and methods

Materials

Mannosylated lipoarabinomannan (ManLAM) from *M. tuberculosis* strain H37Rv was obtained from BEI resources, NIAID, NIH (NR-14848). Lipoarabinomannan from *M. smegmatis* (MsmLAM) was purchased from Labex Corporation, India. Mannotetrose (Man4) and mannoheptose (Man7D1) was procured from Omicron Biochemicals, South Bend, IN. Commercially available PEGRx2 (Condition number 29) from Hampton Research was used for crystallization of native protein. The chemicals for making buffers were obtained from Sigma Aldrich. Most of the other analytical grade chemicals used in this study were purchased from local vendors.

Cloning, expression and purification

Recombinant *Mevo* lectin was expressed and purified from *E. coli* BL21 (DE3) cells as described previously (Sivaji et al. 2017, 2020). Cells were harvested by centrifugation (5500 rpm) and resuspended in Tris-HCl buffer (30-mM Tris-HCl, 300-mM NaCl, 5-mM imidazole, 10% (v/v) glycerol) pH 7.4 containing 5-mM phenylmethylsulfonyl fluoride prior to lysis. Cells were lysed by sonication, total cell lysate was centrifuged at 14000 rpm, and the supernatant loaded directly onto a Ni-NTA column pre-equilibrated with lysis buffer. *Mevo* lectin was eluted with lysis buffer containing 300 mM imidazole. Pure fractions containing *Mevo* lectin were pooled and subjected to size-exclusion chromatography using Superdex-200 column (GE Healthcare, Chicago, IL). Fractions corresponding to homogeneous, *Mevo* lectin were pooled and concentrated using Millipore Centricon up to 10 mg mL^{-1} concentration. Site-directed mutagenesis was employed to generate D134A mutant using pET21b vector that encodes *Mevo* lectin.

Isothermal titration calorimetry

ITC experiments were performed using a MicroCal PEAQ-ITC (Malvern, Canada) instrument. Protein was dialyzed overnight at 4°C against phosphate buffer saline (PBS; 20 mM anhydrous Na$_2$PO$_4$, 4 mM NaH$_2$PO$_4$·2H$_2$O, 150 mM NaCl, pH 7.4) before each titration. *Mevo* lectin was loaded into the calorimeter at concentrations ranging from 10 to 100 μM and titrated with 0.4–2 μL injections (0.2–1 μL for Man7D1) of sugar ligand solution until saturation occurred. Control experiments were performed by titrating ligands into protein-free dialysis buffer. Ligand concentrations used in titrations were 2 mM for Man4, 1 mM
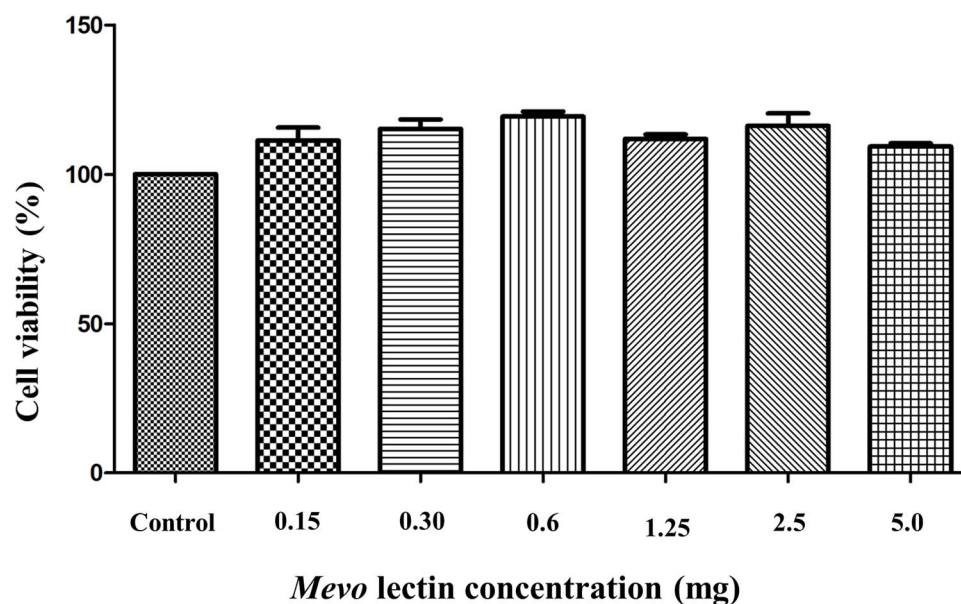
Fig. 7. Cytotoxicity of *Mevo* lectin toward HEK293 cells by means of the MTT colorimetric assay. All values are expressed as mean ± standard error of mean of three independent experiments. MTT, 3-(4,5-dimethylthiazol-2-yl)-2,5-diphenyl tetrazolium bromide.

for Man7D1, 30 µM for ManLAM and 500 µM for MsmLAM. In total, 280 µL of the *Mevo* lectin solution was loaded into the sample cell and the ligand sample was filled in the injection syringe and added to the sample cell as a series of injections separated by 120 seconds interval with constant stirring at 750 rev min⁻¹. The results were analyzed using the MicroCal PEAQ-ITC software. Lipoarabinomannans (ManLAM and MsmLAM) molecular weights were taken from the studies reported elsewhere (Petzold et al. 2005; Kaur et al., 2008). The data were fitted using a one-site model (two sets of sites model for Man7D1), which yielded stoichiometry (n), change in enthalpy (ΔH) and dissociation constant (K_d). The change in entropy (ΔS) was determined using equation $\Delta G = \Delta H - T\Delta S$, where $\Delta G = -RT \ln K_a$, T is the absolute temperature and R = 8.314 J mol⁻¹ K⁻¹. The reported results are the average of three independent titrations for Man7D1, ManLAM, and average of two independent titrations in case of Man4 and MsmLAM at 25°C.

Mannotetrose structure generation and modeling

The mannotetrose (αMan(1,2)αMan(1,2)αMan(1,2)αMan) structure was prepared using CarbBuilder (Kuttel et al. 2016). Docking studies were carried out using Schrodinger suite. Ligands were docked onto one of the subunits of *Mevo* lectin. The docked poses were verified with respect to the D1 arm of *Mevo* lectin complex with Man7D1 to ensure the relative positions of the docked mannotetrose.

Crystallization and data collection

Attempts to cocrystallize the lectin with Man7D1 did not succeed. Eventually, the complex was prepared by soaking the form-2 crystals of the protein (Sivaji et al. 2017, 2020) in a solution containing Tacsimate pH 6.0, 0.1 M MES monohydrate pH 6.0 and 25% (w/v) polyethylene glycol 4000, supplemented with 1 mM of Man7D1 for 12 h. X-ray diffraction data from the crystals of the complex were collected at 100 K at a home source using MAR345 image plate mounted on a Bruker-AXS Microstar Ultra II rotating-anode

generator employing Cu-Kα radiation. Ethylene glycol was used as cryoprotectant. Diffraction images were processed and merged using iMosflm (Battye et al. 2011) and SCALA of the CCP4 program suite (Winn et al. 2011). Structure factor amplitudes were obtained from intensities using TRUNCATE (French and Wilson 1978). Solvent content was estimated using Matthews' method (Matthews, 1968).

Structure solution, refinement and validation

The structure was solved by using molecular replacement with Phaser (McCoy et al. 2007) employing coordinates of a native *Mevo* lectin structure (PDB code: 7BSB) as the search model. REFMAC5 (Murshudov et al. 2011) was used for structure refinement. A few rounds of initial rigid body refinement were followed by refinement of atomic coordinates and B factors with tight noncrystallographic symmetry restraints corresponding to the 7-fold symmetry of the molecule. These restraints were progressively relaxed during the final stages of refinement. COOT (Emsley and Cowtan 2004) was used for model building during iterative cycles of refinement. Ligand molecules were located using difference Fourier maps when R_{work} and R_{free} values were 26 and 29%, respectively. The Man7D1 structure was prepared using CarbBuilder (Kuttel et al. 2016) and PRODRG was used to generate the topology file for the sugar (CCP4 program suite). Fourier difference maps clearly revealed the location of the bound Man7D1. However, partial or no density was observed for the mannose moiety of the D3 arm of Man7D1 and only six mannose residues comprising D1 and D2 arms were modeled into the ligand electron density. The locations were later confirmed using simulated annealing omit maps using CNS v.1.3 (Brunger et al. 1998, 2007). During final refinement cycles, water O atoms were added successively on the basis of peaks with heights greater than 3σ in F_o-F_c maps and greater than 1σ in $2F_o$-F_c maps. A few ethylene glycol molecules were modeled into the electron density where appropriate. The structure was validated using PROCHECK (Laskowski et al. 1993) and MolProbity (Chen et al. 2010). Statistics pertaining to data collection and final results of refinement are given in Table II.
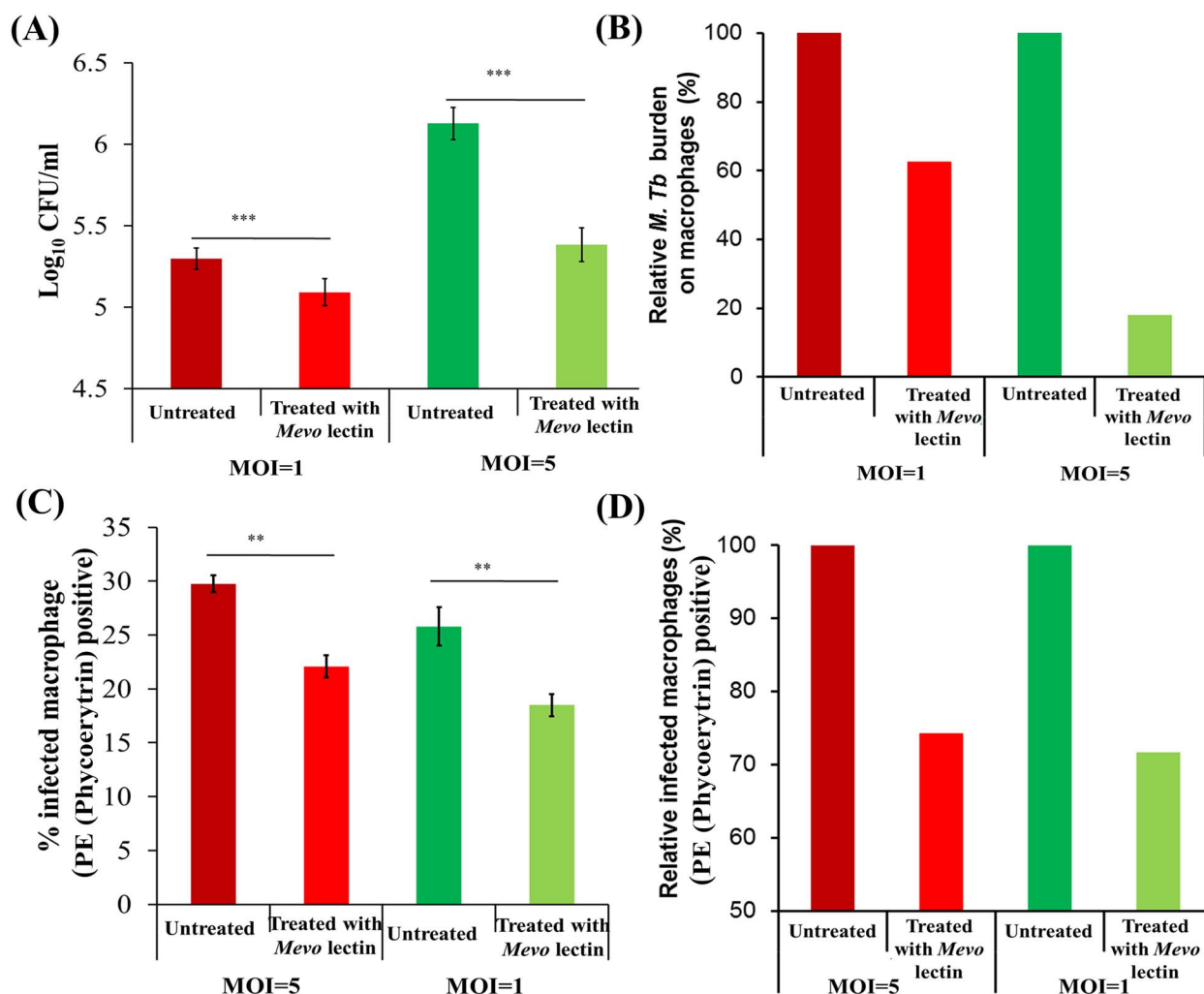
(A)

(B)

(C)

(D)

Fig. 8. Effect of *Mevo* lectin on inhibition of phagocytic uptake of *M. tuberculosis* inside macrophage measured by (**A** and **B**) colony-forming unit (CFU) measurement and (**C** and **D**) flow cytometric analysis. *M. tuberculosis* cells expressing Td-tomato were incubated in presence and absence of *Mevo* lectin (~7 µM) for 1 h. Differentiated THP-1 macrophages were infected with bacilli for 2 h followed by killing of extracellular bacilli by amikacin treatment 2 h. Cells were fixed with PFA and scored for Td-tomato positives using fluorescence-activated cell sorting. In a parallel set macrophages were lysed to release bacilli for CFU enumeration. Ten-fold serial dilutions were plated on 7H11 agar containing OADC (oleic acid; albumin; dextrose; catalase; saline). Error bars represent standard deviations from the mean. ∗∗$P \leq 0.01$; ∗∗∗$P \leq 0.001$. MOI, multiplicity of infection.

Analysis of structures

Figures for molecular representations were generated by using PyMOL (DeLano, 2002). Inter-atomic distances were calculated using CONTACT of the CCP4 program suite. Hydrogen bonds were assigned based on the criteria that the distance between the donor (D) and acceptor (A) atoms was less than or equal to 3.6 Å and D–H . . . A angle was greater than 90°. Structural alignments were done using ALIGN (Cohen, 1997).

In vitro cytotoxicity of *Mevo* lectin on HEK293 cell line using MTT assay

HEK293 cells were procured from National Centre for Cell Sciences (NCCS) Pune, India. These cells were grown in Dulbecco's Modified Eagle's medium with 10% Fetal Bovine Serum (FBS), 1% (v/v) glutaMAX, 100 I.U. mL^{-1} penicillin and streptomycin maintained in a humidified 5% CO_2 at 37°C. A total of 1×10^4 cells mL^{-1} cells

in 100 µL were seeded in a 96 well plate. After 24 h, different concentrations of *Mevo* lectin (0.15-5 mg) were added to the cells. Untreated cells were used as a negative control. MTT (3-(4,5-dimethylthiazol-2-yl)-2,5-diphenyl tetrazolium bromide) reagent (0.5 mg mL^{-1}) was added after 48 h. After 2 h of incubation at 37°C, the MTT reagent was removed and dimethyl sulphoxide (100 µL) was added to each well and the absorbance was then determined by an ELISA reader at a wavelength of 595 nm (Faheina-Martins et al. 2012). The cell viability was calculated from the ratio of the absorbance of the sample wells and control wells, % survival = live cell number (test)/live cell number (control) × 100.

Media and culture conditions

M. tuberculosis strain harboring pTEC27 plasmid (pMSP12:tdTomato) was previously generated in laboratory as described (Tyagi et al. 2020). Bacteria were grown in hygromycin (50 µg mL^{-1}) containing

7H9 broth and 7H11 agar media supplemented with (albumin, dextrose and saline) and (oleic acid, albumin, dextrose, catalase and saline), respectively, to mid-exponential phase ($OD_{600} = 0.4$–0.8) for infection. Human monocytic THP-1 cell line was grown in RPMI1640 media (Cell Clone) supplemented with 10% heat-inactivated FBS. Cells were grown up to maximum 3–5 passages. A total of 3×10^5 cells/well was seeded in a 24 well plate. Cells were differentiated with 20 ng mL^{-1} PMA for 18–20 h before adding to multiwell plate, followed by recovery period of 48 h to differentiate.

Inhibition of phagocytic uptake of bacilli assay

M. tuberculosis tdTomato strain was incubated with 50 μM *Mevo* lectin dissolved in PBS (pH 7.0) or only PBS (control) for 1 h followed by washing to remove unbound compound just before infection. For these studies, a single concentration of the protein used in MTT assay for monitoring cytotoxicity was used in these studies. PMA differentiated cell line THP-1 was infected with mycobacteria (*Mevo* lectin treated or control) for 2 h at MOI of 1 or 5. After 2 h, to kill extracellular bacteria, 50 μg mL^{-1} amikacin (purchased from HiMedia Labs: Cat. No. CMS644) was added, followed by additional 2 h incubation. Postincubation cells were washed thrice with sterile PBS to remove extracellular or dead bacteria.

Flow cytometric analysis to determine relative phagocytic uptake bacilli

Infected Mϕs were fixed with 4% paraformaldehyde for at least 15 min at room temperature followed by washing with PBS. Mϕs were detached in PBS by scrapping and analyzed for the presence of tdTomato using flow cytometer (BD Biosciences). Relative abundance of tdTomato population compared to untreated control is represented.

Measurement of phagocytosed bacilli inside Mϕs

Post incubation with *M. tuberculosis* cells, infected THP-1 macrophage were washed thrice with prewarmed PBS to remove debris, followed by lysis with 0.06% sodium dodecyl sulphate (SDS). Released bacteria were serially diluted 10-fold and plated on 7H11 agar plates. Plates were incubated for 3–4 weeks at 37°C for colonies to appear followed by counting to enumerate number of viable bacilli.

PDB references

Mevo lectin complex with Man7D1 (7DED).

Supplementary data

Supplementary data are available at *Glycobiology* online.

Conflict of interest statement

The authors have no conflicts of interest

Funding

Abbreviations

ITC, isothermal titration calorimetry; PDB, protein data bank; Man7D1, αMan(1,2)αManα(1,2)αMan(1,3)[αMan(1,3)[αMan(1,6)]αMan(1,6)]αMan; mannotriose, αMan(1,3)αMan(1,6)Man; Man4, αMan(1,2)αMan(1,2)αMan(1,3)αMan; mannopentose, αMan(1,3)(αMan(1,6)[αMan(1,6)(αMan(1,3)]-Man; MTT, 3-(4,5-dimethylthiazol-2-yl)-2,5-diphenyl tetrazolium bromide; ManLAM, lipoarabinomannan from *Mycobacterium tuberculosis*; MsmLAM, lipoarabinomannan from *Mycobacterium smegmatis*; CFU, colony-forming unit; Mϕs, macrophages; DCs, dendritic cells; MOI, multiplicity of infection.

Acknowledgments

References

Abhinav KV, Samuel E, Vijayan M. 2016. Archeal lectins: An identification through a genomic search. *Proteins*. 84:21–30.

Abhinav KV, Sharma A, Vijayan M. 2013. Identification of mycobacterial lectins from genomic data. *Proteins*. 81:644–657.

Abhinav KV, Sharma K, Swaminathan CP, Surolia A, Vijayan M. 2015. Jacalin-carbohydrate interactions: Distortion of the ligand molecule as a determinant of affinity. *Acta Crystallogr D Biol Crystallogr*. 71:324–331.

Acosta MP, Lepenies B. 2019. Bacterial glycans and their interactions with lectins in the innate immune system. *Biochem Soc Trans*. 47:1569–1579.

Akkouh O, Ng TB, Singh SS, Yin C, Dan X, Chan YS, Pan W, Cheung RC. 2015. Lectins with anti-HIV activity: A review. *Molecules*. 20:648–668.

Battye TG, Kontogiannis L, Johnson O, Powell HR, Leslie AG. 2011. iMOS-FLM: A new graphical interface for diffraction-image processing with MOSFLM. *Acta Crystallogr D Biol Crystallogr*. 67:271–281.

Borrebaeck CAK, Carlsson R. 1989. Lectins as mitogens. *Adv Lectin Res*. 2:10–27.

Boyd MR, Gustafson KR, McMahon JB, Shoemaker RH, O'Keefe BR, Mori T, Gulakowski RJ, Wu L, Rivera MI, Laurencot CM, et al. 1997. Discovery of cyanovirin-N, a novel human immunodeficiency virus-inactivating protein that binds viral surface envelope glycoprotein gp120: Potential applications to microbicide development. *Antimicrob Agents Chemother*. 41:1521–1530.

Brunger AT, Adams PD, Clore GM, DeLano WL, Gros P, Grosse-Kunstleve RW, Jiang JS, Kuszewski J, Nilges M, Pannu NS, et al. 1998. Crystallography and NMR system: A new software suite for macromolecular structure determination. *Acta Crystallogr D Biol Crystallogr*. 54:905–921.

Brunger AT. 2007. Version 1.2 of the crystallography and NMR system. *Nat Protoc*. 2:2728–2733.

Chen VB, Arendall WB, Headd JJ, Keedy DA, Immormino RM, Kapral GJ, Murray LW, Richardson JS, Richardson DC. 2010. MolProbity: All-atom structure validation for macromolecular crystallography. *Acta Crystallogr D Biol Crystallogr*. 66:12–21.

Cohen GH. 1997. ALIGN: A program to superimpose protein coordinates, accounting for insertions and deletions. *J Appl Cryst*. 30:1160–1161.

Covés-Datson EM, King SR, Legendre M, Gupta A, Chan SM, Gitlin E, Kulkarni VV, Pantaleón García J, Smee DF, Lipka E, et al. 2020. A molecularly engineered antiviral banana lectin inhibits fusion and is efficacious against influenza virus infection *in vivo*. *Proc Natl Acad Sci U S A*. 117:2122–2132.

Dam TK, Fred Brewer C. 2009. Lectins as pattern recognition molecules: The effects of epitope density in innate immunity. *Glycobiology*. 20:270–279.

DeLano WL. 2002. *The PyMOL graphics system*. San Carlos, CA: Delano Scientific.

Drickamer K, Taylor ME. 1993. Biology of animal lectins. *Annu Rev Cell Biol*. 9:237–264.

Driessen NN, Boshoff HI, Maaskant JJ, Gilissen SA, Vink S, van der Sar AM, Vandenbroucke-Grauls CM, Bewley CA, Appelmelk BJ, Geurtsen J. 2012. Cyanovirin-N inhibits mannose-dependent mycobacterium-C-type lectin interactions but does not protect against murine tuberculosis. *J Immunol*. 189:3585–3592.

Ehlers S. 2010. DC-SIGN and mannosylated surface structures of *Mycobacterium tuberculosis*: A deceptive liaison. *Eur J Cell Biol*. 89:95–101.

Emsley P, Cowtan K. 2004. COOT: Model-building tools for molecular graphics. *Acta Crystallogr D Biol Crystallogr*. 60:2126–2132.

Ernst JD. 1998. Macrophage receptors for *Mycobacterium tuberculosis*. *Infect Immun*. 66:1277–1281.

Faheina-Martins GV, da Silveira AL, Cavalcanti BC, Ramos MV, Moraes MO, Pessoa C, Araújo DA. 2012. Antiproliferative effects of lectins from Canavalia ensiformis and Canavalia brasiliensis in human leukemia cell lines. *Toxicol In Vitro*. 26:1161–1169.

Feinberg H, Jégouzo SAF, Rex MJ, Drickamer K, Weis WI, Taylor ME. 2017. Mechanism of pathogen recognition by human dectin-2. *J Biol Chem*. 292:13402–13414.

French S, Wilson K. 1978. On the treatment of negative intensity observations. *Acta Crystallogr Sect A*. 34:517–525.

Fukuda T, Matsumura T, Ato M, Hamasaki M, Nishiuchi Y, Murakami Y, Maeda Y, Yoshimori T, Matsumoto S, Kobayashi K, et al. 2013. Critical roles for lipomannan and lipoarabinomannan in cell wall integrity of mycobacteria and pathogenesis of tuberculosis. *MBio*. 4:e00472–e00412.

Geurtsen J, Chedammi S, Mesters J, Cot M, Driessen NN, Sambou T, Kakutani R, Ummels R, Maaskant J, Takata H, et al. 2009. Identification of mycobacterial alpha-glucan as a novel ligand for DC-SIGN: Involvement of mycobacterial capsular polysaccharides in host immune modulation. *J Immunol*. 183:5221–5231.

Huskens D, Vermeire K, Vandemeulebroucke E, Balzarini J, Schols D. 2008. Safety concerns for the potential use of cyanovirin-N as a microbicidal anti-HIV agent. *Int J Biochem Cell Biol*. 40:2802–2814.

Imberty A, Gerber S, Tran V, Pérez S. 1990. Data bank of three-dimensional structures of disaccharides, a tool to build 3-D structures of oligosaccharides. *Glycoconj J*. 7:27–54.

Imberty A, Pérez S. 2000. Structure, conformation, and dynamics of bioactive oligosaccharides: Theoretical approaches and experimental validations. *Chem Rev*. 100:4567–4588.

Jayaprakash NG, Singh A, Vivek R, Yadav S, Pathak S, Trivedi J, Jayaraman N, Nandi D, Mitra D, Surolia A. 2020. The barley lectin, horcolin, binds high-mannose glycans in a multivalent fashion, enabling high-affinity, specific inhibition of cellular HIV infection. *J Biol Chem*. 295:12111–12129.

Jayaraman S, Eswaramoorthy S, Kumaran D, Swaminathan S. 2005. Common binding site for disialyllactose and tri-peptide in C-fragment of tetanus neurotoxin. *Proteins*. 61:288–295.

Jeyaprakash AA, Srivastav A, Surolia A, Vijayan M. 2004. Structural basis for the carbohydrate specificities of artocarpin: Variation in the length of a loop as a strategy for generating ligand specificity. *J Mol Biol*. 338:757–770.

Ji X, Olinger GG, Aris S, Chen Y, Gewurz H, Spear GT. 2005. Mannose-binding lectin binds to Ebola and Marburg envelope glycoproteins, resulting in blocking of virus interaction with DC-SIGN and complement-mediated virus neutralization. *J Gen Virol*. 86:2535–2542.

Kang PB, Azad AK, Torrelles JB, Kaufman TM, Beharka A, Tibesar E, DesJardin LE, Schlesinger LS. 2005. The human macrophage mannose receptor directs *Mycobacterium tuberculosis* lipoarabinomannan-mediated phagosome biogenesis. *J Exp Med*. 202:987–999.

Kaur D, Obregón-Henao A, Pham H, Chatterjee D, Brennan PJ, Jackson M. 2008. Lipoarabinomannan of mycobacterium: Mannose capping by a multifunctional terminal mannosyltransferase. *Proc Natl Acad Sci U S A*. 105:17973–17977.

Kaus K, Lary JW, Cole JL, Olson R. 2014. Glycan specificity of the *Vibrio vulnificus* hemolysin lectin outlines evolutionary history of membrane targeting by a toxin family. *J Mol Biol*. 426:2800–2812.

Kumari M, Taritla S, Sharma A, Jayabaskaran C. 2018. Antiproliferative and antioxidative bioactive compounds in extracts of marine-derived endophytic fungus *Talaromyces purpureogenus*. *Front Microbiol*. 9:1777.

Kuttel MM, Ståhle J, Widmalm G. 2016. CarbBuilder: Software for building molecular models of complex oligo- and polysaccharide structures. *J Comput Chem*. 37:2098–2105.

Laskowski RA, MacArthur MW, Moss DS, Thornton JM. 1993. PROCHECK: A program to check the stereochemical quality of protein structures. *J Appl Cryst*. 26:283–291.

Loris R. 2002. Principles of structures of animal and plant lectins. *Biochim Biophys Acta*. 572:198–208.

Lusvarghi S, Bewley CA. 2016. Griffithsin: An antiviral lectin with outstanding therapeutic potential. *Viruses*. 8:296.

Matthews BW. 1968. Solvent content of protein crystals. *J Mol Biol*. 33:491–497.

Mazalovska M, Kouokam JC. 2018. Lectins as promising therapeutics for the prevention and treatment of HIV and other potential coinfections. *Biomed Res Int*. 2018:3750646.

McCoy AJ, Grosse-Kunstleve RW, Adams PD, Winn MD, Storoni LC, Read RJ. 2007. Phaser crystallographic software. *J Appl Cryst*. 40: 658–674.

Mitchell CA, Ramessar K, O'Keefe BR. 2017. Antiviral lectins: Selective inhibitors of viral entry. *Antiviral Res*. 142:37–54.

Murshudov GN, Skubák P, Lebedev AA, Pannu NS, Steiner RA, Nicholls RA, Winn MD, Long F, Vagin AA. 2011. REFMAC5 for the refinement of macromolecular crystal structures. *Acta Crystallogr D Biol Crystallogr*. 67:355–367.

Patra D, Mishra P, Surolia A, Vijayan M. 2014. Structure, interactions and evolutionary implications of a domain-swapped lectin dimer from *Mycobacterium smegmatis*. *Glycobiology*. 24:956–965.

Patra D, Mishra P, Vijayan M, Surolia A. 2016. Negative cooperativity and high affinity in chitooligosaccharide binding by a *Mycobacterium smegmatis* protein containing LysM and lectin domains. *Biochemistry*. 55:49–61.

Pérez S, Sarkar A, Rivet A, Breton C, Imberty A. 2015. Glyco3d: A portal for structural glycosciences. *Methods Mol Biol*. 1273:241–258.

Petzold CJ, Stanton LH, Leary JA. 2005. Structural characterization of Lipoarabinomannans from *Mycobacterium tuberculosis* and *Mycobacterium smegmatis* by ESI mass spectrometry. *J Am Soc Mass Spectrom*. 16:1109–1116.

Schlesinger LS. 1993. Macrophage phagocytosis of virulent but not attenuated strains of *Mycobacterium tuberculosis* is mediated by mannose receptors in addition to complement receptors. *J Immunol*. 150:2920–2930.

Sharon N. 2007. Lectins: Carbohydrate-specific reagents and biological recognition molecules. *J Biol Chem*. 282:2753–2764.

Singh DD, Saikrishnan K, Kumar P, Surolia A, Sekar K, Vijayan M. 2005. Unusual sugar specificity of banana lectin from *Musa paradisiaca* and its probable evolutionary origin. Crystallographic and modelling studies. *Glycobiology*. 15:1025–1032.

Singh SS, Devi SK, Ng TB. 2014. Banana lectin: A brief review. *Molecules*. 19:18817–18827.

Sivaji N, Abhinav KV, Vijayan M. 2017. Crystallization and biochemical characterization of an archaeal lectin from *Methanococcus voltae* A3. *Acta Crystallogr Sect F Struct Biol Commun*. 73:300–304.

Sivaji N, Suguna K, Surolia A, Vijayan M. 2020. Structural and related studies on Mevo lectin from *Methanococcus voltae* A3. The first thorough characterisation of an archeal lectin and its interactions. *Glycobiology*. cwaa063.

Sturtevant JM. 1977. Heat capacity and entropy changes in processes involving proteins. *Proc Natl Acad Sci U S A*. 74:2236–2240.

Swaminathan CP, Nandi A, Visweswariah SS, Surolia A. 1999. Thermodynamic analyses reveal role of water release in epitope recognition by a monoclonal antibody against the human guanylyl cyclase C receptor. *J Biol Chem*. 274:31272–31278.

Swanson MD, Boudreaux DM, Salmon L, Chugh J, Winter HC, Meagher JL, André S, Murphy PV, Oscarson S, Roy R, et al. 2015. Engineering a therapeutic lectin by uncoupling mitogenicity from antiviral activity. *Cell*. 163:746–758.

Tailleux L, Schwartz O, Herrmann JL, Pivert E, Jackson M, Amara A, Legres L, Dreher D, Nicod LP, Gluckman JC, et al. 2003. DC-SIGN is the major *Mycobacterium tuberculosis* receptor on human dendritic cells. *J Exp Med*. 197:121–127.

Tanaka H, Chiba H, Inokoshi J, Kuno A, Sugai T, Takahashi A, Ito Y, Tsunoda M, Suzuki K, Takénaka A, et al. 2009. Mechanism by which the lectin actinohivin blocks HIV infection of target cells. *Proc Natl Acad Sci U S A*. 106:15633–15638.

Tanford C. 1980. *The hydrophobic effect: Formation of micelles and biological membranes*. 2nd ed. New York: Wiley.

Torrelles JB, Azad AK, Schlesinger LS. 2006. Fine discrimination in the recognition of individual species of phosphatidyl- myo -inositol Mannosides from *Mycobacterium tuberculosis* by C-type lectin pattern recognition receptors. *J Immunol*. 177:1805–1816.

Tsai CC, Emau P, Jiang Y, Agy MB, Shattock RJ, Schmidt A, Morton WR, Gustafson KR, Boyd MR. 2004. Cyanovirin-N inhibits AIDS virus infections in vaginal transmission models. *AIDS Res Hum Retroviruses*. 20:11–18.

Turner J, Torrelles JB. 2018. Mannose-capped lipoarabinomannan in *Mycobacterium tuberculosis* pathogenesis. *Pathog Dis*. 76:fty026.

Tyagi P, Pal VK, Agrawal R, Singh S, Srinivasan S, Singh A. 2020. *Mycobacterium tuberculosis* reactivates HIV-1 via exosome-mediated resetting of cellular redox potential and bioenergetics. *MBio*. 11:e03293–e03219.

Vigerust DJ, Ulett KB, Boyd KL, Madsen J, Hawgood S, McCullers JA, . 2007. N-linked glycosylation attenuates H3N2 influenza viruses. *J. Virol*. 81:8593–600.

Vijayan M, Chandra N. 1999. Lectins. *Curr Opin Struct Biol*. 9:707–714.

Wesener DA, Dugan A, Kiessling LL. 2017. Recognition of microbial glycans by soluble human lectins. *Curr Opin Struct Biol*. 44:168–178.

Global tuberculosis report 2019. Geneva: World Health Organization; 2019. WHO/CDS/TB/2019.15'

Winn MD, Ballard CC, Cowtan KD, Dodson EJ, Emsley P, Evans PR, Keegan RM, Krissinel EB, Leslie AG, McCoy A, et al. 2011. Overview of the CCP4 suite and current developments. *Acta Crystallogr D Biol Crystallogr*. 67:235–242.

Xiong S, Fan J, Kitazato K. 2010. The antiviral protein cyanovirin-N: The current state of its production and applications. *Appl Microbiol Biotechnol*. 86:805–812.

Zierke M, Smieško M, Rabbani S, Aeschbacher T, Cutting B, Allain FH, Schubert M, Ernst B. 2013. Stabilization of branched oligosaccharides: Lewis(x) benefits from a nonconventional C-H···O hydrogen bond. *J Am Chem Soc*. 135:13464–13472.

Ziółkowska NE, O'Keefe BR, Mori T, Zhu C, Giomarelli B, Vojdani F, Palmer KE, McMahon JB, Wlodawer A. 2006. Domain-swapped structure of the potent antiviral protein griffithsin and its mode of carbohydrate binding. *Structure*. 14:1127–1135.